Discerning the two $K_1(1270)$ poles in $D^0 \to \pi^+ VP$ decay

G. Y. Wang
School of Physics, Zhengzhou University, Zhengzhou, Henan 450001, China
and Departamento de Física Teórica e IFIC, Centro Mixto Universidad de Valencia—CSIC,
Institutos de Investigacion de Paterna, Apartado 22085, 46071 Valencia, Spain

L. Roca
Departamento de Física, Universidad de Murcia, E-30100 Murcia, Spain

E. Oset
Departamento de Física Teórica e IFIC, Centro Mixto Universidad de Valencia—CSIC,
Institutos de Investigacion de Paterna, Apartado 22085, 46071 Valencia, Spain

(Received 25 July 2019; published 17 October 2019)

Within the chiral unitary approach, the axial-vector resonance $K_1(1270)$ has been predicted to manifest a two-pole nature. The lowest pole has a mass of 1195 MeV and a width of 246 MeV and couples mostly to $K^*\pi$, and the highest pole has a mass of 1284 MeV and a width of 146 MeV and couples mostly to ρK. We analyze theoretically how this double-pole structure can show up in $D^0 \to \pi^+ VP$ decays by looking at the vector-pseudoscalar (VP) invariant mass distribution for different VP channels, exploiting the fact that each pole couples differently to different VP pairs. We find that the final $\bar{K}^*\pi$ and $\rho\bar{K}$ channels are sensible to the different poles of the $K_1(1270)$ resonance and hence are suitable reactions to analyze experimentally the double-pole nature of this resonance.

DOI: 10.1103/PhysRevD.100.074018

I. INTRODUCTION

The standard quark model picture, with baryons of three quarks and mesons made of quark and antiquark, has an undeniable value, putting some order in the large amount of mesons and baryons [1–5]. Among the mesons, the vector states follow quite well the $q\bar{q}$ pattern. Recent studies based on QCD and large N_c behavior give extra support to this picture [6]. Yet, many states, such as low lying scalar mesons, many baryons of $1/2^-$, $3/2^-$ nature and some $1/2^+$ excited baryons, do not follow this pattern and call for more complex structures, many of them qualifying as meson-meson or meson-baryon molecules [7]. Among the meson states, the axial-vector meson states are not so successfully reproduced as the vector ones [1,5]. It is then not so surprising that alternative pictures have emerged, and in [8–10] the chiral unitary approach is used, studying the interaction of vector mesons with pseudoscalars, from where the axial-vector mesons emerge as a consequence of the interaction, leading to dynamically generated states, or states of vector-pseudoscalar molecular nature. What makes the picture most attractive is that many decays and properties of the axial-vector mesons are well reproduced within this picture (see recent works along this line and references therein [11–13]).

One of the novel things of the work of [9] is that two states appeared related to $K_1(1270)$, which coupled differently to the different channels. These states were further studied in [14] in connection with experimental information which provided support for two states, one with 1195 MeV, coupling mostly to $K^*\pi$, and another one with 1284 MeV, coupling mostly to ρK. The two peaks were well differentiated in reactions leading to $K^*\pi$ and ρK in the final state.

With data piling up on weak meson decays at present hadron facilities, it becomes convenient to exploit the potential of such reactions to provide information on the nature of the axial-vector states. Work along these lines for other kind of hadrons in the final state from weak decays of B, D, Λ_b, Λ_c hadrons has been summarized in [15]. In the present work we pay attention to the $D^0 \to \pi^+ VP$ decay, with V a vector meson and P a pseudoscalar one. We shall see that we can relate the rates of production of $K^*\pi$ and ρK, and the differential mass distributions peak at different masses as a consequence of the different weight of each of the two $K_1(1270)$ resonances in each of the reactions. While present experimental information does not allow a precise determination of the strength of the reactions, the relative rate and the shapes are accurately predicted and the

rates are within present experimental reach. We use the results to encourage the experimental community to do a thorough investigation of this problem which can lead to the clear observation of the two $K_1(1270)$ states and important information concerning their nature, and that of the axial-vector mesons by extension.

II. AXIAL-VECTOR MESONS IN THE CHIRAL UNITARY APPROACH

For the sake of completeness, in this section we briefly summarize the chiral unitary approach for the vector-pseudoscalar interaction in s-wave [9,14], where most of the low lying axial-vector resonances are obtained dynamically without the need to include them as explicit degrees of freedom (see Refs. [9,14] for further details and explanations).

We make use of the Bethe-Salpeter approach in order to obtain the unitarized VP scattering amplitudes,

$$T = [1 + V\hat{G}]^{-1}(-V)\vec{\epsilon}\cdot\vec{\epsilon}', \tag{1}$$

which effectively sums the diagrammatic series expressed in Fig. 1. In Eq. (1), $\vec{\epsilon}$ and $\vec{\epsilon}'$ stand for the vector-meson polarizations and T is a matrix whose element T_{ij} accounts for the scattering amplitude between the VP channels i and j, with i and j running for the different VP channels allowed for a given isospin, I, strangeness, S, and G-parity. For the present work we are mostly interested in the $I = 1/2$, $S = 1$ case for which the allowed VP channels are $K^*\pi$, ρK, ωK, ϕK, and $K^*\eta$. But we will also need in the final VP interaction the channels with $I = 1$, $S = 0$ which can also be classified by its G-parity, contributing to the $G = +1$ the channels $\phi\pi$, $\omega\pi$, $\rho\eta$, and $(\bar{K}^*K + K^*\bar{K})/\sqrt{2}$, and to $G = -1$ the channels $\rho\pi$ and $(\bar{K}^*K - K^*\bar{K})/\sqrt{2}$.

In Eq. (1), $\hat{G} = (1 + \frac{1}{3}\frac{q_l^2}{M_l^2})G$ is a diagonal matrix containing the VP loop function for a total incident four-momentum P [equal to $(\sqrt{s}, 0, 0, 0)$ in the center of mass frame]:

$$G_l(\sqrt{s}) = i\int \frac{d^4q}{(2\pi)^4}\frac{1}{(P-q)^2 - M_l^2 + i\epsilon}\frac{1}{q^2 - m_l^2 + i\epsilon}, \tag{2}$$

Using dimensional regularization, the loop function of Eq. (2) takes the form

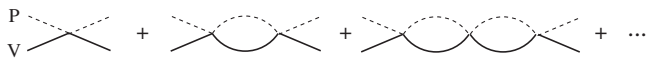

FIG. 1. Diagrammatic representation of the resummation of loops in the unitarization procedure of the VP interaction.

$$\begin{aligned} G_l(\sqrt{s}) = \frac{1}{16\pi^2}\Bigg\{ & a(\mu) + \ln\frac{M_l^2}{\mu^2} + \frac{m_l^2 - M_l^2 + s}{2s}\ln\frac{m_l^2}{M_l^2} \\ & + \frac{q_l}{\sqrt{s}}[\ln(s - (M_l^2 - m_l^2) + 2q_l\sqrt{s}) \\ & + \ln(s + (M_l^2 - m_l^2) + 2q_l\sqrt{s}) \\ & - \ln(-s + (M_l^2 - m_l^2) + 2q_l\sqrt{s}) \\ & - \ln(-s - (M_l^2 - m_l^2) + 2q_l\sqrt{s})]\Bigg\}, \end{aligned} \tag{3}$$

where $M_l(m_l)$ is the mass of the vector (pseudoscalar) meson, q_l is the on-shell momentum of the meson in the loop, μ is the scale of dimensional regularization, and $a(\mu)$ is a subtraction constant which reabsorbs possible changes in μ so that the model only depends on one free parameter, $a(\mu)$. By fitting to experimental $K^-p \to K^-\pi^+\pi^-p$ data, in Ref. [14] the value $a = -1.85$, for $\mu = 900$ MeV, was obtained, which is indeed of natural size [9]. The effect of the finite width of the vector mesons can be taken into account by folding the loop functions with the vector-meson spectral function

$$S(s_V) = -\frac{1}{\pi}\mathrm{Im}\left\{\frac{1}{s_V - M_V^2 + iM_V\Gamma_V}\right\} \tag{4}$$

such that

$$G_l(\sqrt{s}, M_l, m_l) = \frac{\int_{(M_V-2\Gamma_V)^2}^{(M_V+2\Gamma_V)^2} ds_V G(\sqrt{s}, \sqrt{s_V}, m_l) S(s_V)}{\int_{(M_V-2\Gamma_V)^2}^{(M_V+2\Gamma_V)^2} ds_V S(s_V)} \tag{5}$$

where we have taken a reasonable range, $(M_V \pm 2\Gamma_V)^2$, in the s_V integration.

The other input needed in Eq. (1) are the $VP \to VP$ tree level amplitudes, V_{ij}, which can be obtained from the chiral invariant Lagrangian [9,16]

$$\mathcal{L}_{VVPP} = -\frac{1}{4f^2}\mathrm{Tr}([V^\mu, \partial^\nu V_\mu][P, \partial_\nu P]), \tag{6}$$

where V and P are the usual $SU(3)$ matrices containing vector and pseudoscalar mesons, respectively.

The s-wave projected $VP \to VP$ tree level amplitudes obtained from the Lagrangian of Eq. (6) are

$$\begin{aligned} V_{ij}(s) = -\frac{\epsilon\cdot\epsilon'}{8f^2}C_{ij}[3s - (M_i^2 + m_i^2 + M_j^2 + m_j^2) \\ -\frac{1}{s}(M_i^2 - m_i^2)(M_j^2 - m_j^2)], \end{aligned} \tag{7}$$

with $f = 115$ MeV [14] and C_{ij} are numerical coefficients which are tabulated in [9,14]. The function V entering Eq. (1) is given by Eq. (7) removing the $\epsilon\cdot\epsilon'$ factor.

We have used the lowest order chiral Lagrangian to obtain the potential to be used in the Bethe-Salpeter equation, Eq. (1). In principle, when going to second order in the first loop in Fig. 1, one should add the contribution of the Lagrangians to next order and so on. This is the philosophy of a perturbative approach. In the unitary approach one is resuming infinite orders but certainly one cannot introduce the potential to all orders which is unknown. Yet, there are many reasons that support the use of the lowest order potential and unitarize the amplitude. One of them is that if one includes in the potential the next to leading order and unitarizes, one finds results practically equal to those using the lowest order in the meson-meson interaction [17–20]. One reason to understand this is the findings in [21] that the chiral Lagrangians up to second order are equivalent to the results of the local hidden gauge approach based on the exchange of vector mesons. The exchange of vector mesons omitting the q^2 dependence of the propagators leads to the lowest order Lagrangians. Keeping them reproduces the second order chiral Lagrangian assuming vector-meson dominance. Actually it is easy to see that Eq. (7) can be obtained from vector exchange in the limit of $q^2 = 0$ in the vector propagators. In as much as q^2 can be neglected versus the mass squared of the vector mesons one is consistent with the information of the chiral Lagrangians up to order 2. This is the case when one studies the interaction of mesons relatively close to threshold as we do. The second reason is that in the unitary method one regularizes the loop functions and there is some relative freedom there which is used to obtain one energy of a resonance or some other phenomenological information. One can see in Eq. (1) that there is a trade-off between G and V. Some changes in V can be accommodated by a corresponding change in G. Then the couplings at the poles, which is basically the relevant information, are not changed in this trade-off. There are more examples of the goodness of this approach. In the study of the $\eta \to \gamma\gamma\pi^0$ reaction [22,23] one finds that the unitary approach with the lowest order and a proper regularization can accommodate terms up to order $\mathcal{O}(p^6)$ in the chiral perturbation theory of [24]. Ultimately, it is the fairness of the results to describe many physical processes with this approach that gives support to this picture as can be seen in the review papers [25,26].

On the other hand, note that we have not included explicitly axial-vector resonances in the formalism (by means of Breit-Wigner amplitudes or any other approaches). The axial-vector resonances are actually generated dynamically from the highly nonlinear dynamics involved in the unitary amplitude, Eq. (1), where the only input is the lowest order VP chiral Lagrangian, Eq. (6). Indeed, they show up as poles of the scattering amplitude, Eq. (1), in its second Riemann sheet of the complex center of mass energy, $\sqrt{s}$, plane. For the $(S, I) = (1, 1/2)$ case, two poles are found at $(1195 - i123)$ MeV and $(1284 - i73)$ MeV, where the real part can be identified with the mass and the imaginary part with half the width. In [9,14] these poles were assigned to the experimental $K_1(1270)$ resonance, which therefore would actually correspond to two different resonances. For the $(S, I) = (0, 1)$ with negative G-parity one pole was found in [9] associated to the $a_1(1260)$ and another one with negative G-parity associated to the $b_1(1235)$.

TABLE I. Couplings of the two poles associated to the $K_1(1270)$ resonance to the different VP channels. All the units are in MeV.

	$1195 - i123$		$1284 - i73$	
$\sqrt{s_p}$	g_i	$\lvert g_i\rvert$	g_i	$\lvert g_i\rvert$
ϕK	$2096 - i1208$	2420	$1166 - i774$	1399
ωK	$-2046 + i821$	2205	$-1051 + i620$	1220
ρK	$-1671 + i1599$	2313	$4804 + i395$	4821
$K^*\eta$	$72 + i197$	210	$3486 - i536$	3526
$K^*\pi$	$4747 - i2874$	5550	$769 - i1171$	1401

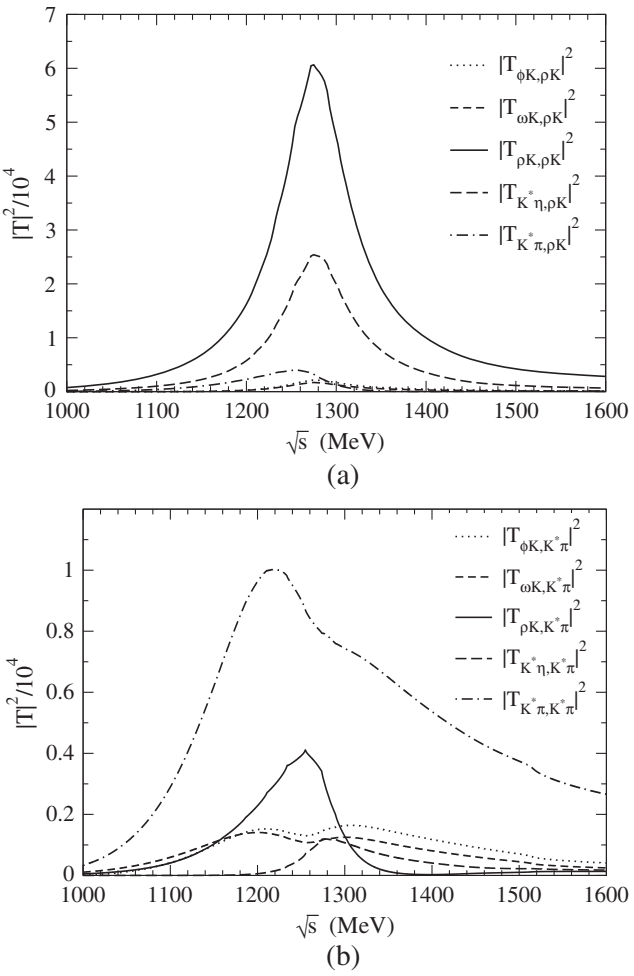

FIG. 2. Modulus squared of the VP scattering amplitudes for $(S, I) = (1, 1/2)$, (a) for ϕK transitions and (b) for $K^*\pi$ transitions.

The couplings, g_i, of the resonances associated to the poles to the ith VP channel can be obtained from the residue of the T_{ij} amplitude at the pole position, $\sqrt{s_p}$, since close to the pole the amplitude T_{ij} in the second Riemann sheet takes the form

$$T_{ij} = \frac{g_i g_j}{s - s_p}. \tag{8}$$

The couplings obtained for $(S, I) = (1, 1/2)$ are shown in Table I. We can see that the lowest mass pole couples mostly to $K^*\pi$ and the highest mass pole couples dominantly to ρK, although the couplings to most of the other channels are also sizable. Therefore we would expect that different reactions weighing differently the $K^*\pi$ and ρK production mechanisms would see different shapes, corresponding to one or the other pole associated to the $K_1(1270)$ resonance [9].

Indeed, in Fig. 2 we show the amplitudes in the real axis, for $(S, I) = (1, 1/2)$, of the different VP channels going to ρK and $K^*\pi$. The effect of the different poles in the shape of the mass distributions for the different channels is clearly visible. For instance, in the $\rho K \to \rho K$ amplitude we can recognize the dominance of the higher mass pole and in the $K^*\pi \to K^*\pi$ channel the lower mass one. This dependence on the final channels of the weight of the different poles is what we expect to observe in the present work in the VP mass distributions in $D^0 \to \pi^+\rho\bar{K}$ and $D^0 \to \pi^+\bar{K}^*\pi$ decays. For $(S, I) = (0, 1)$ channels, the values of the pole positions, the couplings to the different VP channels, and plots for the VP amplitudes can be see in Ref. [9].

III. FORMALISM FOR $D^0 \to \pi^+ VP$ DECAY

A. Tree level production

The dominant contribution to the elementary $D^0 \to \pi^+ VP$ process at the quark level is depicted in Fig. 3. First the charm quark of the D^0 meson produces an s quark and a π^+ through the Cabibbo dominant vertices Wcs and $Wu\bar{d}$. Production of a kaon instead of the pion would imply a Cabibbo suppressed coupling to the W boson. The hadronization, giving rise to a VP final pair, is then implemented with the $^3P_0$ model [27–29], where an extra $\bar{q}q$ with the quantum numbers of the vacuum is produced

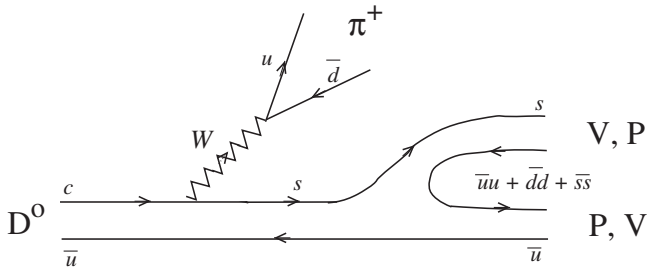

FIG. 3. Elementary $D^0 \to \pi^+ VP$ process at the quark level.

and becomes real thanks to the large phase space available. For the different VP pairs that can be produced, we can determine their relative strength by using the following $SU(3)$ argument:

After the hadronization, the quark flavor final state is given by

$$|H\rangle \equiv |s(\bar{u}u + \bar{d}d + \bar{s}s)\bar{u}\rangle.$$

If we define

$$q \equiv \begin{pmatrix} u \\ d \\ s \end{pmatrix} \quad \text{and} \quad M \equiv q\bar{q}^{\intercal} = \begin{pmatrix} u\bar{u} & u\bar{d} & u\bar{s} \\ d\bar{u} & d\bar{d} & d\bar{s} \\ s\bar{u} & s\bar{d} & s\bar{s} \end{pmatrix}, \tag{9}$$

then the final hadron state can be written as

$$|H\rangle = \sum_{i=1}^{3} |M_{3i} q_i \bar{u}\rangle = \sum_{i=1}^{3} |M_{3i} M_{i1}\rangle = |(M^2)_{31}\rangle. \tag{10}$$

Next we write the $q\bar{q}$ M-matrix in terms of the physical mesons P, or V, as

$$M \Rightarrow P = \begin{pmatrix} \frac{\pi^0}{\sqrt{2}} + \frac{\eta}{\sqrt{3}} + \frac{\eta'}{\sqrt{6}} & \pi^+ & K^+ \\ \pi^- & -\frac{1}{\sqrt{2}}\pi^0 + \frac{\eta}{\sqrt{3}} + \frac{\eta'}{\sqrt{6}} & K^0 \\ K^- & \bar{K}^0 & -\frac{\eta}{\sqrt{3}} + \frac{2\eta'}{\sqrt{6}} \end{pmatrix},$$

or the vector mesons

$$M \Rightarrow V \equiv \begin{pmatrix} \frac{1}{\sqrt{2}}\rho^0 + \frac{1}{\sqrt{2}}\omega & \rho^+ & K^{*+} \\ \rho^- & -\frac{1}{\sqrt{2}}\rho^0 + \frac{1}{\sqrt{2}}\omega & K^{*0} \\ K^{*-} & \bar{K}^{*0} & \phi \end{pmatrix}. \tag{11}$$

P the usual mixing between the singlet and octet to give η and η' [30], and for V the ideal $\omega_1 - \omega_8$ mixing to produce ω and ϕ, has been used in order to agree with the quark content of M in Eq. (9).

The arguments leading to Eq. (10) refer only to flavor. However, we wish to produce a pseudoscalar and a vector and we have two options, the first M in Eq. (10) can correspond to a vector and the second to a pseudoscalar or vice versa. Since the arguments used say nothing about vector or pseudoscalar production from the $q\bar{q}$, the two options appear with the same weight. Thus, in terms of V and P fields, for the final hadronic state we find

$$(VP)_{31} + (PV)_{31} = \frac{1}{\sqrt{2}} K^{*-}\pi^0 + \bar{K}^{*0}\pi^- + \phi K^- + \frac{1}{\sqrt{2}}\rho^0 K^- + \frac{1}{\sqrt{2}}\omega K^- + \bar{K}^0\rho^-, \tag{12}$$

where the $K^{*-}\eta$ channel has mathematically canceled and, as in [9], we neglect the η' because of its large mass. Equation (12) provides the relative weights between the different VP channels in charge basis, and can be converted to VP states in isospin basis with $I = 1/2$, $I_3 = -1/2$, which is the basis used in the previous section, giving rise to

$$\sum_i h_i(V_iP_i)|_{(I=\frac{1}{2},I_3=-\frac{1}{2})} \equiv \sqrt{\frac{3}{2}}\bar{K}^*\pi - \sqrt{\frac{3}{2}}\rho\bar{K} + \frac{1}{\sqrt{2}}\omega\bar{K} + \phi\bar{K}. \quad (13)$$

Taking into account the previous discussion, the tree level amplitude for the $D^0 \to \pi^+ V_i P_i$ decay can then be written as

$$t_i \equiv A h_i, \quad (14)$$

with A a normalization constant. Note, however, that since we have a vector meson in the final state the amplitude must also be proportional to its polarization vector ϵ, which must be contracted with another vector. The other vector must be a momentum of the particles. Taking into account that $\epsilon_\mu p_V^\mu = 0$ from the Lorentz condition and that $p_{D^0} = p_{\pi^+} + p_V + p_P$, we are only left with two independent structures: $\epsilon_\mu p_{\pi^+}^\mu$ and $\epsilon_\mu p_P^\mu$. In addition, we can safely ignore the ϵ^0 component of the vector polarization, which is found to be a very good approximation in these kinds of processes as shown in [31] (see the Appendix A of that reference). Thus, the tree level amplitude will have the structure

$$t_{\text{tree}} = a h_i \vec{\epsilon}\cdot\vec{p}_{\pi^+} + b h_i \vec{\epsilon}\cdot\vec{p}_P, \quad (15)$$

with a and b unknown complex constants which will be determined later on.

B. VP final state interaction

As explained in Sec. II, the two poles for the axial-vector $K_1(1270)$ resonance are dynamically generated from the VP interaction. Therefore we have to implement the final state interaction of the VP pair produced in the elementary $D^0 \to \pi^+ VP$ mechanism of Fig. 3. This is depicted in Fig. 4, where the thick dot represents the VP scattering amplitude accounting for the series of Fig. 1. Actually we will see below that the Fig. 4(b) mechanism will generate the two $K_1(1270)$ poles and the Fig. 4(c) mechanism will only be possible for the $I = 1$ channels that generate $a_1(1260)$ and $b_1(1235)$. Furthermore, note that the tree level Fig. 4(a) mechanism contributes to the a and b terms of Eq. (15), the Fig. 4(b) mechanism only to the a term, and the Fig. 4(c) mechanism only to the b term.

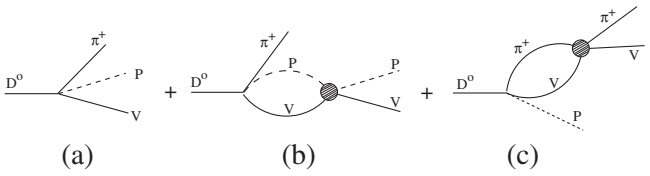

FIG. 4. VP final state interaction (a) tree level, (b) VP rescattering, and (c) $\pi^+ V$ rescattering.

The $D^0 \to \pi^+ VP$ channels for which $K_1(1270)$ is more relevant are those where the allowed VP invariant mass distribution contains or is close to the region of the poles associated to this resonance. The thresholds for the VP channels in $I = 1/2$, $S = 1$, $K^*\pi$, ρK, ωK, ϕK, and $K^*\eta$ are 1032, 1271, 1278, 1515, and 1441 MeV, respectively. Therefore $K^*\pi$, ρK, and ωK are the final channels which contain or are closer to the real part of the two $K_1(1270)$ poles, (1195 and 1284 MeV), and then we expect $K_1(1270)$ to play an important role in those channels. Thus, in the present work we are going to evaluate the channels $D^0 \to \pi^+ \bar{K}^{*0}\pi^-$, $D^0 \to \pi^+\rho^0 K^-$, and $D^0 \to \pi^+\omega K^-$.

The scattering amplitudes, $\mathcal{M}_i$, for the $D^0 \to \pi^+ V_i P_i$ for this process can be written as

$$\begin{aligned}
\mathcal{M}_{D^0\to\pi^+\bar{K}^{*0}\pi^-} &= a\vec{\epsilon}\cdot\vec{p}_{\pi^+}\sqrt{\frac{2}{3}}\left(h_{K^*\pi} + \sum_j h_j G_j T^{I=1/2}_{j,K^*\pi}\right) \\
&\quad + b\vec{\epsilon}\cdot\vec{p}_{\pi^-}\sqrt{\frac{2}{3}}h_{\bar{K}^*\pi}, \\
\mathcal{M}_{D^0\to\pi^+\rho^0 K^-} &= a\vec{\epsilon}\cdot\vec{p}_{\pi^+}\left(\frac{-1}{\sqrt{3}}\right)\left(h_{\rho\bar{K}} + \sum_j h_j G_j T^{I=1/2}_{j,\rho\bar{K}}\right) \\
&\quad + b\vec{\epsilon}\cdot\vec{p}_{K^-}\left(\frac{-1}{\sqrt{3}}\right)h_{\rho\bar{K}}\left(1 + \frac{1}{2}G_{\rho\pi}T^{I=1}_{\rho\pi,\rho\pi}\right), \\
\mathcal{M}_{D^0\to\pi^+\omega K^-} &= a\vec{\epsilon}\cdot\vec{p}_{\pi^+}\left(h_{\omega\bar{K}} + \sum_j h_j G_j T^{I=1/2}_{j,\omega\bar{K}}\right) \\
&\quad + b\vec{\epsilon}\cdot\vec{p}_{K^-}(h_{\omega\bar{K}} + h_{\omega\bar{K}}G_{\omega\pi}T^{I=1}_{\omega\pi,\omega\pi} \\
&\quad + h_{\phi K}G_{\phi\pi}T^{I=1}_{\phi\pi,\omega\pi}),
\end{aligned} \quad (16)$$

with h_i the coefficients defined in Eq. (13), G_i the same VP loop function of Eq. (5), and the index j running for all possible different VP channels. The superindex in the VP amplitudes T_{ij} stands for the total isospin. Again, a folding with the vector-meson spectral function is implemented for G_j.

For the VP unitarized amplitudes T_{ji} one should in principle use the amplitudes obtained from Eq. (1) (see again Fig. 2). But in an actual experimental analysis one typically would try to fit Breit-Wigner like shapes for the resonance and then one would use something more similar to Eq. (8). Therefore, in Eq. (16), we can also approximate the T_{ji} amplitudes by Eq. (8) and then use, for $I = 1/2$, $S = 1$,

$$T_{ji} = T^A_{ji} + T^B_{ji}, \tag{17}$$

where the superindex A stands for the amplitude of Eq. (8) for the lowest mass $K_1(1270)$ pole and the superindex B for the highest mass pole. Similarly for the $I = 1$, $S = 0$, amplitudes we can use Breit-Wigner shapes as in Eq. (8). Note that the closer the poles are to the real axis the better this approximation is, and it is exact at the poles. For $I = 1$, where the unitarized amplitudes generate dynamically the $a_1(1260)$ and $b_1(1235)$ resonances, we use instead the Breit-Wigner shapes with couplings from [9] and masses and widths from the Particle Data Group (PDG) [32].

The amplitudes of Eq. (16) are of the form

$$\mathcal{M}_i = A\vec{\epsilon}\cdot\vec{p}_{\pi^+} + B\vec{\epsilon}\cdot\vec{p}_P. \tag{18}$$

For the evaluation of the $D^0 \to \pi^+ V_i P_i$ decay width we will have to perform the sum over polarizations of the modulus squared, $\sum|\mathcal{M}_i|^2$, which gives

$$\sum|\mathcal{M}_i|^2 = |A|^2\vec{p}^{\,2}_{\pi^+} + |B|^2\vec{p}^{\,2}_P + 2\mathrm{Re}(AB^*)\vec{p}_{\pi^+}\cdot\vec{p}_P, \tag{19}$$

with $\vec{p}_{\pi^+}$ and $\vec{p}_P$ the momentum of the π^+ and the pseudoscalar P_i in the D_0 rest frame. From Eq. (19), the invariant mass distributions $\frac{d\Gamma(D^0\to\pi^+V_iP_i)}{dM_{V_iP_i}}$ and $\frac{d\Gamma(D^0\to\pi^+V_iP_i)}{dM_{V_i\pi^+}}$ are readily obtained after integrating over one invariant mass the double differential mass distribution [32]

$$\frac{d^2\Gamma(D^0\to\pi^+V_iP_i)}{dM_{V_iP_i}dM_{V_i\pi^+}} = \frac{1}{8(2\pi)^3M^3_{D^0}}\sum|\mathcal{M}_i|^2 M_{V_iP_i}M_{V_i\pi^+}. \tag{20}$$

In order to take into account the finite width of the final vector meson, a folding with the vector-meson spectral function, analogous to the one in Eq. (5), is implemented for the invariant mass distributions. Indeed, for the ρ vector meson, the threshold of the $\rho\bar{K}$ mass distribution is very close to the position of the two $K_1(1270)$ poles and then the tail of the ρ meson is very relevant.

The amplitudes in Eq. (16) depend on the complex a and b constants. We can take a real because of an unobservable global phase, and then we are left with three unknown parameters: a, $|b|$, and ϕ_b, with ϕ_b the phase of b. We could in principle determine these parameters from experimental $D^0 \to \pi^+ V_i P_i$ branching ratios data in the PDG [32]. However, we cannot use experimental data for $\mathrm{BR}(D^0 \to \pi^+ V_i P_i)$ coming from an intermediate $K_1(1270)$ since it is incompatible with our model because the experimental analyses are performed assuming that there is only one $K_1(1270)$ pole instead of the two obtained in our theory. Therefore we are only left with the following available experimental information in the PDG [32]: First the branching ratio $\mathrm{BR}(D^0 \to \pi^+\rho^0 K^-) = (6.87 \pm 0.31)\%$, from which we have to subtract $\mathrm{BR}(D^0 \to \bar{K}^{*0}\rho^0; \bar{K}^{*0} \to K^-\pi^+) = (1.01 \pm 0.05)\%$ since that channel does not contribute to the mechanism of Fig. 3. We will call that subtracted value $BR_1 \equiv \widetilde{\mathrm{BR}}(D^0 \to \pi^+\rho^0 K^-) = (5.86 \pm 0.31)\%$. The other experimental datum we can use from the PDG [32] is $\mathrm{BR}(D^0 \to \pi^+\omega K^-) = (3.1 \pm 0.6)\%$, from which we have to subtract $\frac{2}{3}\mathrm{BR}(D^0 \to \bar{K}^{*0}\omega) = \frac{2}{3}(1.1 \pm 0.5)\%$, which we will call $BR_2 \equiv \widetilde{\mathrm{BR}}(D^0 \to \pi^+\omega K^-) = 2.4 \pm 0.7\%$. With two data and three parameters there could be mathematically infinitely many solutions, but that would not be a problem if they turned out to lay on a narrow range of values. Actually, in the present case for the concrete data explained above, we do not find an exact mathematical solution for the central values of the experimental BR_1 and BR_2 but there is a solution within the uncertainty range of the experimental data. In order to get this solution we minimize the chi-squared function

$$\chi^2 = \left(\frac{BR_1^{\mathrm{exp}} - BR_1^{\mathrm{th}}}{\sigma_{BR_1}}\right)^2 + \left(\frac{BR_2^{\mathrm{exp}} - BR_2^{\mathrm{th}}}{\sigma_{BR_2}}\right)^2, \tag{21}$$

where the labels "exp" and "th" stand for the experimental and theoretical values and σ_{BR_i} are the experimental uncertainties mentioned above. We get a minimum value of $\chi^2 = 0.26$ at $a = 3.13\ \mathrm{GeV}^{-1}$, $b = 5.47e^{1.74\pi i}\ \mathrm{GeV}^{-1}$ for which $BR_1 = 5.82\%$ and $BR_2 = 2.75\%$, well within the range allowed by the uncertainties of the experimental values. We could as well have fitted a and b using the unitary amplitudes for T_{ji}. Similar results arise that do not modify the shape of the distributions. Note, indeed, that in the present work we are specially interested in the shape of the invariant mass distribution to see the different shape of the two distinct poles of $K_1(1270)$ and the global normalization is a collateral aspect. Anyway, the difference between using Breit-Wigner or unitarized amplitudes is well within the 50% uncertainty that we will assume for our reults, as will be explained below in the results section.

IV. RESULTS

In Figs. 5(a), 5(c), and 5(e) we show the VP invariant mass distribution for the $\bar{K}^{*0}\pi^-$, $\rho^0 K^-$, and ωK^- final VP channels considering the contribution of different mechanisms. The different curves are explained and discussed below. The curves labeled "unitarized" are the results considering for the $T^{I=1/2}_{ij}$ amplitudes in Eq. (16) the full unitarized amplitudes from Eq. (1). The curves labeled "BW poles" are the results using, in Eq. (16), for the final VP amplitude in $I = 1/2$ the explicit double Breit-Wigner like shape, Eq. (17) instead of Eq. (1). For the latter case, we also show the contribution considering only the lowest mass pole (A) or the highest mass pole (B) in the Breit-Wigner-like amplitude $T^{I=1/2}_{ij}$ in Eq. (16). Finally, the curve labeled "background" represents the results removing, in Eq. (16), the $T^{I=1/2}_{ij}$ amplitude, i.e., the $K_1(1270)$ contribution.

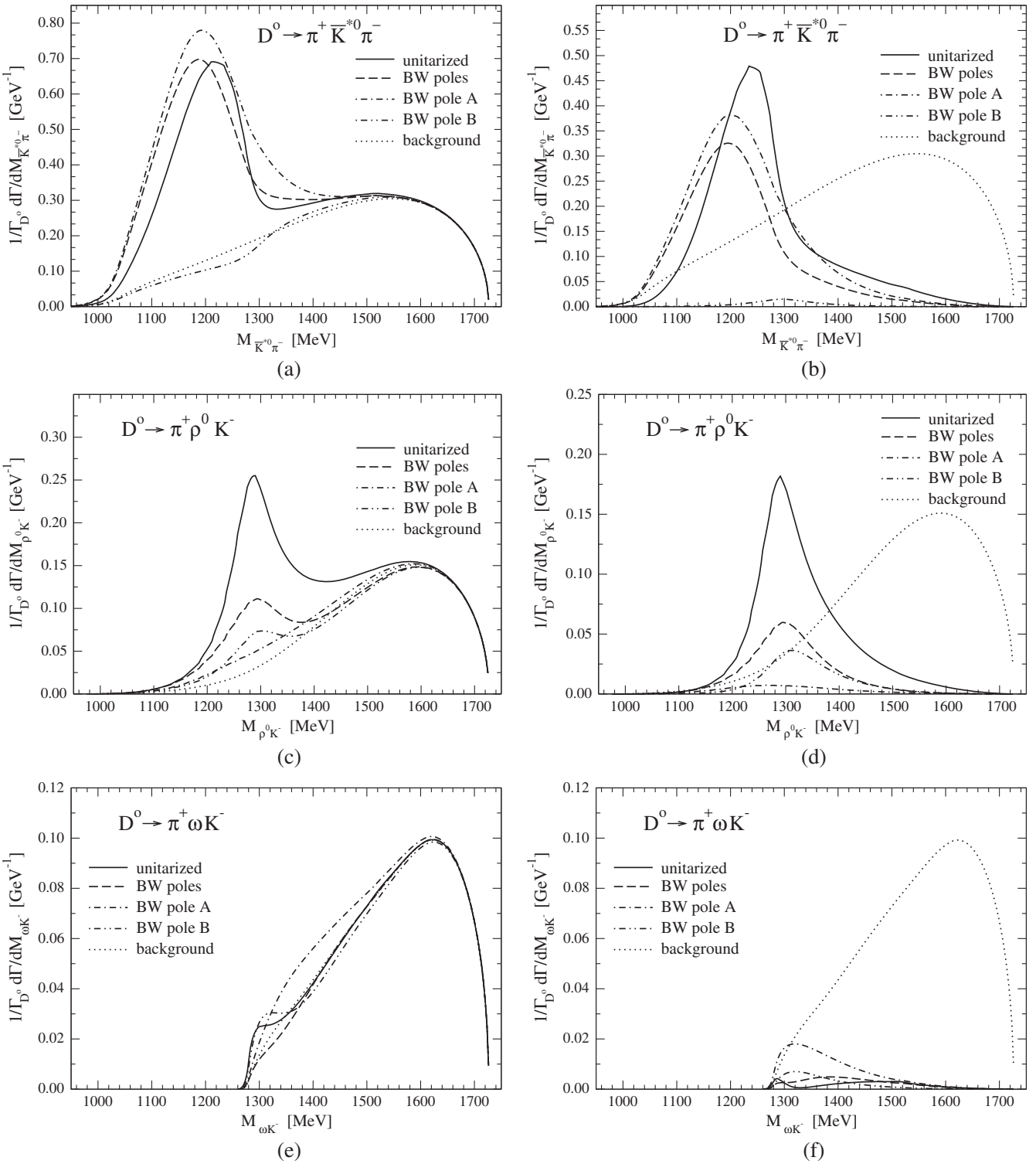

FIG. 5. VP invariant mass distribution in the $D^0 \to \pi^+ VP$ decay for $D^0 \to \pi^+ \bar{K}^{*0}\pi^-$, $D^0 \to \pi^+\rho^0 K^-$ and $D^0 \to \pi^+\omega K^-$. (a),(c),(e) consider the interaction with the tree level elementary mechanism of Fig. 3. (b),(d),(f) are without the interference with the background contributions. Further explanations are in the text.

First we can clearly appreciate the $K_1(1270)$ resonant effects in the shape of the curves since they differ with respect to the one considering only the background production, [only the Fig. 4(a) and 4(c) diagrams]. Note also that the available phase space does not start at just $m_V + m_P$, because of the finite width of the vector meson. This is more relevant for the $\rho\bar{K}$ channel. Next we can compare the result using for the final state interaction

in $I = 1/2$ the full unitarized amplitudes with the result using the explicit double Breit-Wigner-like shape, Eq. (17). The difference is not qualitatively very relevant in the position of the peaks observed. The main physical difference is that the unitarized amplitude in the real axis not only accounts for the possible resonance contributions but also provides the full VP scattering amplitude in $I = 1/2$, which then does not necessarily have a Breit-Wigner-like shape, or a combination of them. However, in an actual experiment, the resonance would be defined more similarly to a Breit-Wigner (or two if the double-pole nature is to be considered) and then an experimental analysis of the $K_1(1270)$ contribution should obtain something more similar to the "BW poles" curve in the figures. Next, by looking at the contributions considering only the lowest mass pole (A) or the highest mass pole (B), in the Breit-Wigner-like amplitude of Eq. (17), we see that in the $D^0 \to \pi^+ \bar{K}^{*0} \pi^-$ channel the pole A clearly dominates the bump in the mass distribution. This is reminiscent of the large coupling of the lowest mass pole to $K^*\pi$, Table I. For the $D^0 \to \pi^+ \rho^0 K^-$ channel it is worth noting that the available phase space starts close to the $K_1(1270)$ poles and then the allowed phase space in this region is smaller than for the $\bar{K}^*\pi$ case. Even still, we can appreciate a clear bump closer to the pole B. However, the analysis is a bit more involved because of subtle interference effects with the tree level contribution: Indeed, in Figs. 5(b), 5(d), and 5(f) we show also the same results as in Figs. 5(a), 5(c), and 5(e) but considering only the contribution from the $I = 1/2$ VP scattering amplitude, [i.e., considering only the Fig. 4(b) mechanism]. This would be the case if one could ideally filter the $K_1(1270)$ contribution. In this case the pole B clearly dominates the distribution and we can see more clear resonance shapes for the individual pole contributions.

In Fig. 6 the full results (solid line) using the unitarized $I = 1/2$ amplitude and the other contributions added coherently, as in Eq. (16), are compared with the full result but are adding the background incoherently (dashed line), i.e., the sum of curves "unitarized" and "background" in Figs. 5(b), 5(d), and 5(f). We see that the coherent interference with the background has an important repercussion in the final shape of the distribution. Therefore an experimental analysis should take into account a coherent interference between their $K_1(1270)$ resonance amplitudes and a background term. Actually the most important effect is the interference of the unitarized amplitude with the constant term, see the first line in Eq. (16). The result considering only the $GT^{I=1/2}$ terms in Eq. (16) (curve labeled "only GT" in Fig. 6) is also compared to the result adding the constant in front of the sum symbol in Eq. (16) (curve labeled "only 1+GT" in Fig. 6). We see that the position and shape of the $K_1(1270)$ peaks are clearly distorted. This conclusion is also applicable to the other channels. The important role played by similar interferences with tree level mechanisms in other reactions is also

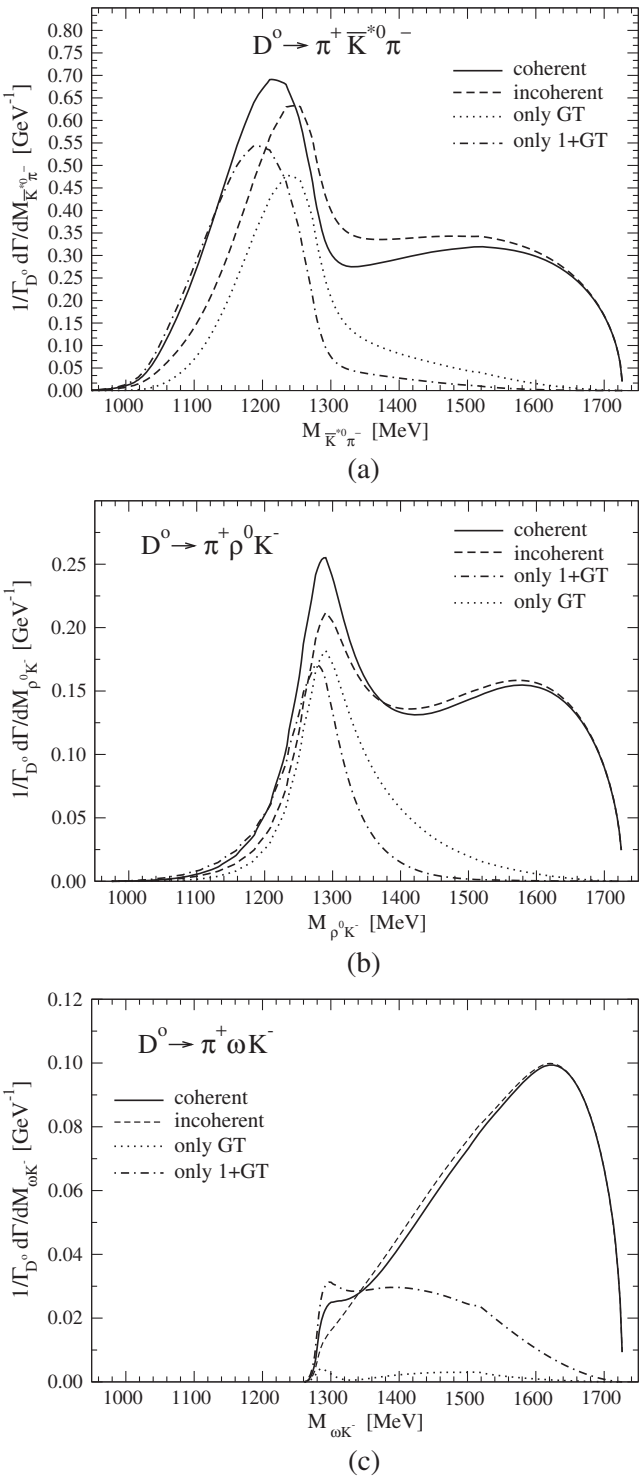

FIG. 6. VP invariant mass distribution in the $D^0 \to \pi^+ VP$ decay for $D^0 \to \pi^+ \bar{K}^{*0} \pi^-$ (a), $D^0 \to \pi^+ \rho^0 K^-$ (b), and $D^0 \to \pi^+ \omega K^-$ (c). Solid line, full results using the unitarized $I = 1/2$ amplitude with the other contributions added coherently; dashed line, same but adding the background incoherently.

discussed in [13,33]. We can understand why the position and width of the apparent peak differs from the one obtained if one does not consider the interference with

TABLE II. Different contributions to the branching ratios for $D^0 \to \pi^+ VP$ decay. The results in parenthesis are without the background mechanisms. Pole $A(B)$ means that the $B(A)$ pole are removed from the model. (See the further explanation in the text.) All the results are in %.

	Unitarized	BW poles	Pole A	Pole B	Background
$\bar{K}^{*0}\pi^-$	23 (8.6)	26 (6.6)	28 (8.6)	14 (0.24)	14
$\rho^0 K^-$	7.9 (2.7)	5.8 fit (0.97)	5.3 (0.19)	5.1 (0.57)	4.8
ωK^-	2.8 (0.07)	2.8 fit (0.10)	3.0 (0.28)	2.8 (0.088)	2.8

the tree level. If we consider only one channel, for simplicity, the structure $1 + GT$ of Eq. (16) is

$$1 + GT = -\frac{T}{V}, \tag{22}$$

but V has a zero close but below threshold and then T/V tends to accumulate strength in the lowest part of the spectrum and then the resonance appears at lower energies and a bit wider than what is obtained if the interference with the tree level is not considered.

In the $D^0 \to \pi^+ \omega K^-$ channel the available phase space is in principle similar to the $\rho^0 K^-$ channel but the mass distribution does not benefit from the large width of the ρ meson and then the phase space starts more abruptly at $m_\omega + m_K = 1278$ MeV. However, an accumulation of strength is still visible at the lowest part of the spectrum close to the $K_1(1270)$ poles. However, in this observable both poles are responsible for the accumulation of strength because, although the coupling to ωK is larger for pole A, it is further away in energy and then pole B still has a large contribution. Furthermore, there is strong interference between the amplitudes of both poles.

From the previous results on the invariant mass distributions we can conclude that $D^0 \to \pi^+ \bar{K}^* \pi$ is the best suited channel to study the lowest mass $K_1(1270)$ pole and $D^0 \to \pi^+ \rho \bar{K}$ the highest mass one, although both poles should be taken into account and the coherent interference with a nonresonant tree level production must be considered.

In Table II we show the different contributions to the integrated branching ratios (in percent) for the different $D^0 \to \pi^+ VP$ channels. The values in the parenthesis are the results removing the background mechanisms. Note that the results depend on the a and b coefficients of Eq. (15), which, as explained in Sec. II, are obtained from experimental data which has an error of about 30%. Therefore we can assign to our theoretical results, in Fig. 5 and Table II, a conservative uncertainty of about 50%.

In the PDG [32] and [34] there are some experimental branching ratios which could in principle be compared to ours. However, all fits to data in the experimental works are based on the existence of a unique $K_1(1270)$ resonance. Should the fits be done assuming explicitly two K_1 resonances, with different mass and width and different couplings to $K^*\pi$ and ρK, the output would certainly be different and, hence, any attempt to compare our results with these experimental ones can only lead to confusion. The value of the present work is that it makes clear predictions for very different shapes with $K^*\pi$ and ρK in the final states. According to this, the optimal way to proceed from an experimental point of view would be, first, to test whether these predictions are correct, and in the positive case proceed to redo fits to data including explicitly two K_1 resonances that sum coherently, and background terms in the amplitudes that can interfere with the resonances.

V. SUMMARY

We have studied theoretically the suitability of the $D^0 \to \pi^+ VP$ decay to check the double-pole nature of the $K_1(1270)$ resonance predicted by the chiral unitary approach. Indeed, with the only input of the lowest order chiral perturbation theory Lagrangians for the VP interaction and the implementation of unitarity in coupled channels, it was obtained in [9,14] that the $K_1(1270)$ corresponds actually to two poles located at $(1195 - i123)$ and $(1284 - i73)$ MeV in the second Riemann sheet of the VP scattering amplitudes, without the need to include the poles as explicit degrees of freedom: They appear naturally from the nonlinear dynamics involved in the unitarization procedure. Each pole couples differently to different VP channels and therefore one would expect that reactions weighing the mechanisms producing different VP channels differently would be more influenced by one pole or the other. This is the situation in the present case where we have implemented the final state interaction in the elementary VP pair produced in the $D^0 \to \pi^+ VP$ tree level process, where the different channels are related by $SU(3)$. We have found that the $\bar{K}^*\pi$ mass distribution in the $D^0 \to \pi^+ \bar{K}^* \pi$ channel is clearly dominated by the lowest mass pole and the $D^0 \to \pi^+ \rho \bar{K}$ channel by the highest mass pole, although the interference between both poles is relevant. This is a consequence of the reactions peaking at different VP invariant masses. We have also discussed the important role played by the coherent interference with the tree level mechanism which should be considered in an experimental analysis in order to properly extract the resonance properties. Devoted experimental studies of this reaction could help to shed light on the double-pole structure of this resonance.

ACKNOWLEDGMENTS

This work is partly supported by the Spanish Ministerio de Economia y Competitividad and European FEDER funds under Contracts No. FIS2017-84038-C2-1-P B and No. FIS2017-84038-C2-2-P B, and the Generalitat Valenciana in the program Prometeo II-2014/068, and the project Severo Ochoa of Instituto de Fisica Corpuscular (IFIC), SEV-2014-0398 (E. O.). This work is partly supported by the National Natural Science Foundation of China under Grants No. 11505158 and No. 11847217. It is also supported by the Academic Improvement Project of Zhengzhou University. G. Y. W. wishes to acknowledge the support from Zhengzhou University in the program of visiting abroad for Ph.D. students.

[1] S. Godfrey and N. Isgur, Phys. Rev. D **32**, 189 (1985).
[2] N. Isgur and G. Karl, Phys. Rev. D **18**, 4187 (1978).
[3] S. Capstick and N. Isgur, Phys. Rev. D **34**, 2809 (1986); AIP Conf. Proc. **132**, 267 (1985).
[4] S. Capstick and W. Roberts, Prog. Part. Nucl. Phys. **45**, S241 (2000).
[5] J. Vijande, F. Fernandez, and A. Valcarce, J. Phys. G **31**, 481 (2005).
[6] J. R. Pelaez, Phys. Rep. **658**, 1 (2016).
[7] F. K. Guo, C. Hanhart, U. G. Meissner, Q. Wang, Q. Zhao, and B. S. Zou, Rev. Mod. Phys. **90**, 015004 (2018).
[8] M. F. M. Lutz and E. E. Kolomeitsev, Nucl. Phys. **A730**, 392 (2004).
[9] L. Roca, E. Oset, and J. Singh, Phys. Rev. D **72**, 014002 (2005).
[10] Y. Zhou, X. L. Ren, H. X. Chen, and L. S. Geng, Phys. Rev. D **90**, 014020 (2014).
[11] W. H. Liang, S. Sakai, and E. Oset, Phys. Rev. D **99**, 094020 (2019).
[12] L. R. Dai, L. Roca, and E. Oset, Phys. Rev. D **99**, 096003 (2019).
[13] S. J. Jiang, S. Sakai, W. H. Liang, and E. Oset, arXiv: 1904.08271.
[14] L. S. Geng, E. Oset, L. Roca, and J. A. Oller, Phys. Rev. D **75**, 014017 (2007).
[15] E. Oset *et al.*, Int. J. Mod. Phys. E **25**, 1630001 (2016).
[16] M. C. Birse, Z. Phys. A **355**, 231 (1996).
[17] J. A. Oller, E. Oset, and J. R. Pelaez, Phys. Rev. D **59**, 074001 (1999); **60**, 099906(E) (1999); **75**, 099903(E) (2007).
[18] Z. H. Guo and J. A. Oller, Phys. Rev. D **84**, 034005 (2011).
[19] J. R. Pelaez and G. Rios, Phys. Rev. D **82**, 114002 (2010).
[20] J. R. Pelaez and G. Rios, Phys. Rev. Lett. **97**, 242002 (2006).
[21] G. Ecker, J. Gasser, H. Leutwyler, A. Pich, and E. de Rafael, Phys. Lett. B **223**, 425 (1989).
[22] E. Oset, J. R. Pelaez, and L. Roca, Phys. Rev. D **67**, 073013 (2003).
[23] E. Oset, J. R. Pelaez, and L. Roca, Phys. Rev. D **77**, 073001 (2008).
[24] L. Ametller, J. Bijnens, A. Bramon, and F. Cornet, Phys. Lett. B **276**, 185 (1992).
[25] J. A. Oller, E. Oset, and A. Ramos, Prog. Part. Nucl. Phys. **45**, 157 (2000).
[26] E. Oset *et al.*, Int. J. Mod. Phys. E **25**, 1630001 (2016).
[27] L. Micu, Nucl. Phys. **B10**, 521 (1969).
[28] A. Le Yaouanc, L. Oliver, O. Pene, and J. C. Raynal, Phys. Rev. D **8**, 2223 (1973).
[29] E. Santopinto and R. Bijker, Phys. Rev. C **82**, 062202 (2010).
[30] A. Bramon, A. Grau, and G. Pancheri, Phys. Lett. B **283**, 416 (1992).
[31] S. Sakai, E. Oset, and A. Ramos, Eur. Phys. J. A **54**, 10 (2018).
[32] M. Tanabashi *et al.* (Particle Data Group), Phys. Rev. D **98**, 030001 (2018).
[33] L. Roca, J. E. Palomar, E. Oset, and H. C. Chiang, Nucl. Phys. **A744**, 127 (2004).
[34] M. Ablikim *et al.* (BESIII Collaboration), Phys. Rev. D **95**, 072010 (2017).